# Molecular Analysis of Base Damage Clustering Associated with a Site-Specific Radiation-Induced DNA Double-Strand Break

Author(s): Kamal Datta, Pawel Jaruga, Miral Dizdaroglu, Ronald D. Neumann, and Thomas A. Winters
Source: Radiation Research, 166(5):767-781. 2006.
Published By: Radiation Research Society
DOI: http://dx.doi.org/10.1667/RR0628.1
URL: http://www.bioone.org/doi/full/10.1667/RR0628.1

RADIATION RESEARCH **166**, 767–781 (2006)
0033-7587/06 $15.00


# Molecular Analysis of Base Damage Clustering Associated with a Site-Specific Radiation-Induced DNA Double-Strand Break

Kamal Datta,[a] Pawel Jaruga,[b,c] Miral Dizdaroglu,[b] Ronald D. Neumann[a] and Thomas A. Winters[a,1]

[a] *Department of Nuclear Medicine, Warren Grant Magnuson Clinical Center, National Institutes of Health, Bethesda, Maryland;* [b] *Chemical Science and Technology Laboratory, National Institute of Standards and Technology, Gaithersburg, Maryland; and* [c] *Department of Chemical and Biochemical Engineering, University of Maryland Baltimore County, Baltimore, Maryland*

**Datta, K., Jaruga, P., Dizdaroglu, M., Neumann, R. D. and Winters, T. A. Molecular Analysis of Base Damage Clustering Associated with a Site-Specific Radiation-Induced DNA Double-Strand Break. *Radiat. Res.* 166, 767–781 (2006).**

**Base damage flanking a radiation-induced DNA double-strand break (DSB) may contribute to DSB complexity and affect break repair. However, to date, an isolated radiation-induced DSB has not been assessed for such structures at the molecular level. In this study, an authentic site-specific radiation-induced DSB was produced in plasmid DNA by triplex forming oligonucleotide-targeted $^{125}$I decay. A restriction fragment terminated by the DSB was isolated and probed for base damage with the *E. coli* DNA repair enzymes endonuclease III and formamidopyrimidine-DNA glycosylase. Our results demonstrate base damage clustering within 8 bases of the $^{125}$I-targeted base in the DNA duplex. An increased yield of base damage (purine > pyrimidine) was observed for DSBs formed by irradiation in the absence of DMSO. An internal control fragment 1354 bp upstream from the targeted base was insensitive to enzymatic probing, indicating that the damage detected proximal to the DSB was produced by the $^{125}$I decay that formed the DSB. Gas chromatography-mass spectrometry identified three types of damaged bases in the ~32-bp region proximal to the DSB. These base lesions were 8-hydroxyguanine, 8-hydroxyadenine and 5-hydroxycytosine. Finally, evidence is presented for base damage >24 bp upstream from the $^{125}$I-decay site that may form via a charge migration mechanism.** © 2006 by Radiation Research Society

## INTRODUCTION

DNA double-strand breaks (DSBs) are recognized as the most biologically severe primary lesions produced by radiation (*1–3*). Numerous studies over several decades have implicated radiation-induced DSBs as the lesion responsible for most radiation cytotoxicity (*2, 4–10*), yet due to the stochastic nature of DSB formation by beam irradiation, the structural organization of an isolated radiation-induced DSB has not been determined directly at the molecular level. This issue is becoming increasingly important in light of recent studies suggest not only that DSB repairability may be a function of structure (*11–13*) but also that human cells may invoke a specialized DSB-repair sub-pathway to repair structurally complex DSBs (*14*).

Mammalian cells repair most DSBs via the nonhomologous end-joining (NHEJ) pathway. The ''core'' proteins involved in NHEJ were identified by genetic means in the absence of detailed structural information about the DSB lesions with which they interact (*15, 16*). This is contrary to other DNA repair pathways in which lesions were identified and the enzymatic activities required to effect their repair were then determined (*17*). Prior knowledge of the DNA lesion being acted upon permits a rational approach to understanding the basic biochemical requirements necessary for the pathway that acts to repair the damage. This has not been the case for NHEJ. Therefore, a more complete understanding of the enzymatic requirements and mechanisms needed to repair radiation-induced DSBs necessitates a more detailed understanding of the structural characteristics that define these lesions.

To address this issue, we have employed a method using $^{125}$I-labeled triplex-forming oligonucleotides (TFO) to create authentic radiation-induced DSBs site-specifically in plasmid DNA. The ability of TFOs to enter the major groove of DNA and sequence-specifically hybridize to a polypurine tract within the duplex allows precise positioning of the radionuclide within that sequence (*18, 19*). Coupled with the unique decay characteristics of $^{125}$I (*20*), which produces DSBs within about one helical turn of the decay site at an efficiency of ~1 DSB per decay (*18, 21*) that exhibit biological characteristics that mimic DSBs induced by high-LET beam radiation (*22, 23*), we were able to generate sufficiently large quantities of DSBs similar to those induced by high-LET radiation at a known sequence position to permit analysis of the break structure.

Previously, we used this approach to assess DSB-associated AP site clustering by repair enzyme-mediated probing of short restriction fragments terminated by the $^{125}$I-

[1] Address for correspondence: Nuclear Medicine Department, Warren Grant Magnuson Clinical Center, National Institutes of Health, Bldg. 10, Room 1C401, 9000 Rockville Pike, Bethesda, MD 20892; e-mail: twinters@mail.cc.nih.gov.

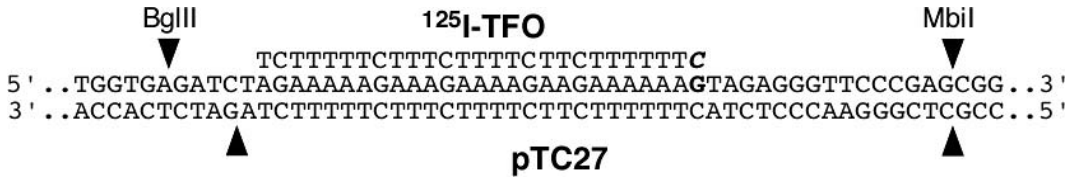


**FIG. 1.** Plasmid pTC27. The plasmid target sequence aligned with the $^{125}$I-TFO and restriction sites used to obtain smaller fragments for analysis. The 5-[$^{125}$I]-dC of the TFO is indicated in bold italics, and the ''G'' residue of the plasmid duplex targeted for Hoogsteen base pairing by the TFO is indicated in bold.

induced DSB end (*24*). We found AP site clustering within ~8 bp of the DSB end as a high-frequency consequence of DSB formation and found that their formation is largely due to direct radiation effects and non-radiation ''hot atom'' type effects associated with neutralization of the highly positively charged (~+21) $^{125}$Te daughter atom formed by $^{125}$I decay and transmutation (*25–29*).

Here we address the question of base damage clustering produced in association with DSB formation by using the same DNA substrates employed for the AP site study and enzymatically probing them with the *E. coli* DNA repair enzymes endonuclease III (endo III) and formamidopyrimidine-DNA glycosylase (Fpg). These enzymes recognize pyrimidine- and purine-derived DNA base lesions, respectively (*30–34*). Our results indicate a high degree of base damage clustering that again occurs within ~8 bp of the DSB end. Unlike our findings for AP sites in these substrates, the yield of DSB-associated base damage was strongly influenced by the presence or absence of the radical scavenger DMSO, indicating a role for scavengeable free radicals during base damage formation. In addition, we identified three specific base lesions (8-hydroxyguanine, 8-hydroxyadenine and 5-hydroxycytosine) by GC/MS analysis of the DSB terminated restriction fragments.

## MATERIALS AND METHODS

### *Materials*

Reagents for oligonucleotide synthesis were obtained from Glen Research (Sterling, VA). Dynabeads M-280, magnetic beads conjugated to streptavidin, were purchased from Dynal A.S. (Oslo, Norway). T4 polynucleotide kinase (T4 PNK), calf intestinal alkaline phosphatase (CIAP), exo$^-$ Klenow enzyme, and all restriction enzymes except *Stu*I (NEB; Beverly, MA) and *Sfi*I (Invitrogen, Carlsbad, CA) were from Fermentas (Hanover, MD). γ-$^{32}$P-ATP, α-$^{32}$P-dCTP, α-$^{32}$P-dATP and 5-[$^{125}$I]-dCTP were obtained from Perkin Elmer Life Science (Boston, MA). DNA repair enzymes were from Trevigen (Gaithersburg, MD). CL-4B Sepharose and G-50 and G-25 Sephadex spin columns were obtained from Amersham Pharmacia Biotech (Piscataway, NJ). Plasmid pTC27 was a generous gift from Dr. Michael Seidman (NIA, Baltimore, MD). *Escherichia coli* strain DH10B was obtained from Invitrogen (Carlsbad, CA).

### *TFO Synthesis and Purification*

A pyrimidine-motif TFO (27 mer) was synthesized and $^{125}$I-labeled by primer extension as described previously (*19, 35*). Primer (5′-TCTTTTCTTTCTTTTCTTCTTTTTT-3′) and biotinylated template (5′-CCCGAAAAAAGAAGAAAAGAAAGAAAAAGACCCCCBCCCB-3′) oligonucleotides were synthesized on an ABI-394 DNA/RNA synthesizer (Applied Biosystems, Foster City, CA) and band-purified after 12% denaturing PAGE. A primer/template duplex (molar ratio of 1:1.5) was formed by incubating the oligos in exo$^-$ Klenow buffer (10 m*M* Tris-HCl, pH 7.5, 5 m*M* $MgCl_2$, 7.5 m*M* DTT) at 90°C for 3 min followed by gradual cooling to room temperature. Exo$^-$ Klenow enzyme (1 U) was used for primer extension in the presence of 455 pmol 5-[$^{125}$I]-dCTP [(81,400 GBq/mmol) dCTP:primer ratio, 2:1] at room temperature for 30 min. The reaction was stopped by addition of EDTA to a final concentration of 10 m*M*. Unincorporated 5-[$^{125}$I]-dCTP was removed by Sephadex G-50 spin column chromatography, and the $^{125}$I-TFO was isolated by heat denaturation of the duplex after binding to streptavidin-labeled magnetic Dynabeads. Dynabead-bound template was removed in an ice-cold magnet and purified $^{125}$I-TFO was recovered in the supernatant.

### *Triplex Formation/Damage Induction*

The plasmid pTC27 containing a 27-bp polypurine sequence, which permits binding of a pyrimidine-motif TFO, was used to create triplexes (Fig. 1). Triplex formation was achieved by mixing topoisomerase I relaxed (Promega, Madison, WI) pTC27 and $^{125}$I-TFO (plasmid:TFO ratio of 1:1.5) in binding buffer (30 m*M* $NaCH_3COOH$, pH 4.5, 10 m*M* $MgCl_2$, and 1 m*M* spermidine) and incubating at 70°C for 3 min followed by gradual cooling to room temperature. Unbound TFO was removed by CL-4B Sepharose spin column chromatography. The $^{125}$I-triplex bound plasmid sample was divided into two equal parts, and both were adjusted to a final volume of 1 ml in 1× binding buffer with one of the two samples being brought to 2 *M* DMSO. The triplex samples were then stored at −80°C for 1 month to accumulate damage.

### *DSB Substrate Preparation*

Substrate for repair enzyme probing was prepared as described previously (*24*) by gel purification and electroelution of pTC27 plasmid DNA linearized by $^{125}$I-TFO decay-mediated DSB induction. The linear DNA was $^{32}$P end-labeled directly at the DSB end using T4 PNK or *Taq* DNA polymerase (5′- or 3′-labeling of the DSB end, respectively) followed by cutting with *Bgl*II. Alternatively, the plasmid was cut with *Bgl*II first, then labeled at the restriction enzyme cut end using T4 PNK or exo$^-$ Klenow fragment DNA polymerase (5′- or 3′-end labeling, respectively). Specific end-labeling conditions have been described in detail previously (*24*). Cleavage of the damaged pTC27 DNA with *Bgl*II generates a series of small fragments from the upstream side of the DSB site ranging from 29 bp to 35 bp as measured with respect to the 5′-end of the restriction fragment upper strand (due to the variable break site position resulting from $^{125}$I decay). The $^{125}$I target position is located 32 bp downstream from the *Bgl*II upper strand cleavage site and corresponds to the 3′-most G of the plasmid's polypurine triplex binding site (Fig. 1).

The small *Bgl*II fragments were isolated and quantitatively purified from the remaining large plasmid fragment by Sepharose CL-4B spin column chromatography as described previously (*36*). Using this method, the small fragments were recovered with ≥99% purity and used as substrates for enzymatic probing of base damage. A 49-bp fragment obtained from a region of the damaged linear DNA 1354 bp upstream from the $^{125}$I-TFO target site and a 47-bp *Bgl*II/*Mbi*I fragment from undamaged

plasmid that spans the triplex/damage target site were used as background and negative controls, respectively.

### *Repair Enzyme Probing*

The end-labeled DSB damage-terminated substrates as well as control substrates were enzymatically probed for the presence of base damage with *E. coli* endo III and Fpg. Damaged and control substrates were treated with 3 U of each repair enzyme for 90 min at 37°C in 10 m*M* Hepes-KOH, pH 7.4, 100 m*M* KCl in a final volume of 10 μl [enzyme activities were equivalent under these conditions (data not shown)]. The reaction products were mixed with an equal volume of formamide loading buffer and run in 20% denaturing polyacrylamide-sequencing gels. Gels were visualized with a Fuji 1500 phosphorimager, and the grayscale image density for each sample lane was obtained with Fuji Science Lab ImageGauge v3.45 software (Stamford, CT).

### *GC/MS Analysis*

Purified *Bgl*II fragments were also subjected to GC/MS analysis as described previously (*37, 38*) to confirm the presence of base damage and determine specific chemical identities of base lesions present in the fragments. The 47-bp *Bgl*II/*Mbi*I fragment purified from undamaged plasmid was used as a background control. Results were expressed as a ratio of base damage in the DSB damaged fragments to the background damage observed in the undamaged control fragment.

### *Data Analysis and Quality Control*

*Gel image analysis*. Autoradiographic analysis and band quantification were performed as follows. Multiple independent determinations of the banding patterns obtained for the damaged DNA oligos (either enzyme-treated or not) were performed for each scavenging condition and for each end-labeling method. In most cases three experiments were done; however, in three cases, only two experiments were done. The number of iterations of the experiments is indicated on a case-by-case basis in the legends of the figures. The digital autoradiographic grayscale-image-density data obtained from each lane of each experiment was subjected to Gaussian deconvolution followed by nonlinear peak fitting using PeakFit for Windows v4 (SPSS Inc., Chicago, IL). The deconvolved and fitted peak areas were then used to determine the percentage area that each band (in the enzymatically treated and untreated lanes) represented as a function of the total peak area observed for the damaged DNA control lanes (untreated by enzyme) in each experiment. Finally, the mean percentage density (as a function of total peak area) and standard error of the mean were determined for the density of each band observed for each irradiation condition and end-labeling method. The mean percentage density of each fragment was then plotted along with error bars indicating the SEM (Figs. 2–5). These values are reported as ''Relative Band Density (percentage area)'' in the figures.

*Enzyme quality control*. Enzyme preparations were assessed for nonspecific endonuclease and exonuclease activities by running control enzyme assays in parallel with the assays done to assess for base damage in our damaged DNA substrates. Representative results of the control assays are shown in Fig. 2B, lanes 9–11. These control assays were performed at the same time as the experimental assays using the same method. The control substrate is a 47-mer duplex oligo with the same sequence as the fragment defined by the *Bgl*II/*Mbi*I restriction fragment of plasmid pTC27 (Fig. 1). No degradation of the 47-mer control oligo was observed, indicating that the enzyme preparations were free of nonspecific endonuclease and exonuclease activities as well as 5′-phosphatase activity under our assay conditions. Similar assays were performed with each new batch of enzyme concurrent with or prior to its use in analysis of damaged DNA substrates.

*Loading controls*. Lane-to-lane loading variability in our assay was estimated as a function of density variation between the lanes containing the undamaged 47-mer duplex oligonucleotide control substrate that had been either treated or untreated with endo III or Fpg (examples are presented in Fig. 2B, lanes 9–11). These control assays were performed using the same enzyme reaction method and run in parallel with the experimental analyses on the same gel. Therefore, variations between the band densities of the untreated control oligo and the bands observed for the third of the reaction mixture subjected to endo III or Fpg treatment reflect loading variability (i.e., the enzymes do not cleave the control oligo). Using this approach, we have determined the lane-to-lane loading variability in our assays to be an average of 4.1% with a standard deviation of ±3.7% calculated from a total of 14 determinations for endo III and an average of 6.2% ± 3.6% for Fpg (calculated from 13 determinations).

## RESULTS

Base damage produced in association with radiation-induced DSB formation was investigated by enzymatic probing of a short DNA restriction fragment isolated from the upstream side of a site-specific radiation-induced DSB. The DSB terminated restriction fragment (29–35 bp) was probed with *E. coli* endo III and Fpg to reveal pyrimidine- and purine-derived base lesions, respectively. In addition to establishing the presence and distribution of base damage relative to the DSB, base lesions were identified and quantified by GC/MS.

Endo III is a DNA glycosylase with an associated AP lyase activity that exhibits broad substrate specificity for pyrimidine-derived lesions and a single purine-derived lesion, i.e. 4,6-diamino-5-formamidopyrimidine (*31*). Upon recognition of a damaged base, endo III cleaves the *N*-glycosyl bond between the damaged base and the sugar moiety, forming an AP site that is cleaved by lyase-mediated β-elimination (*31–33, 39, 40*). Fpg catalyzes a similar reaction at a broad range of purine-derived lesions, except Fpg's associated DNA lyase facilitates β–δ elimination at the AP site (*41, 42*). Fpg also exhibits low-level activity at some pyrimidine-derived lesions when incorporated in oligonucleotides as single lesions (*30, 32, 34*). Thus the end result of endo III or Fpg activity at a damaged base is a strand break, and use of these enzymes permitted differential probing for pyrimidine- or purine-derived lesions in the $^{125}$I-DSB-terminated *Bgl*II restriction fragments.

### *Endo III and Fpg Probing of the 5′-End-Labeled Upper Strand*

The 5′-end-labeled upper strand of the damaged DNA fragments exhibited only modest endo III sensitivity, as expected for this purine-rich sequence (Fig. 2B, lanes 4 and 7, and panels C and D). In the *Bgl*II fragment sample obtained from DNA irradiated in the presence of DMSO [(+) DMSO], endo III cleavage was limited and occurred only in fragments close to the DSB maximum (fragments $A_5$ and $A_6$; Fig. 2C). In comparison, the (−) DMSO sample displays a broader range of endo III-sensitive fragments, with cleavage detectable in fragments $T_3$ through $A_8$ (Fig. 2D). The net density reduction resulting from endo III treatment was more than twofold greater for the (−) DMSO sample

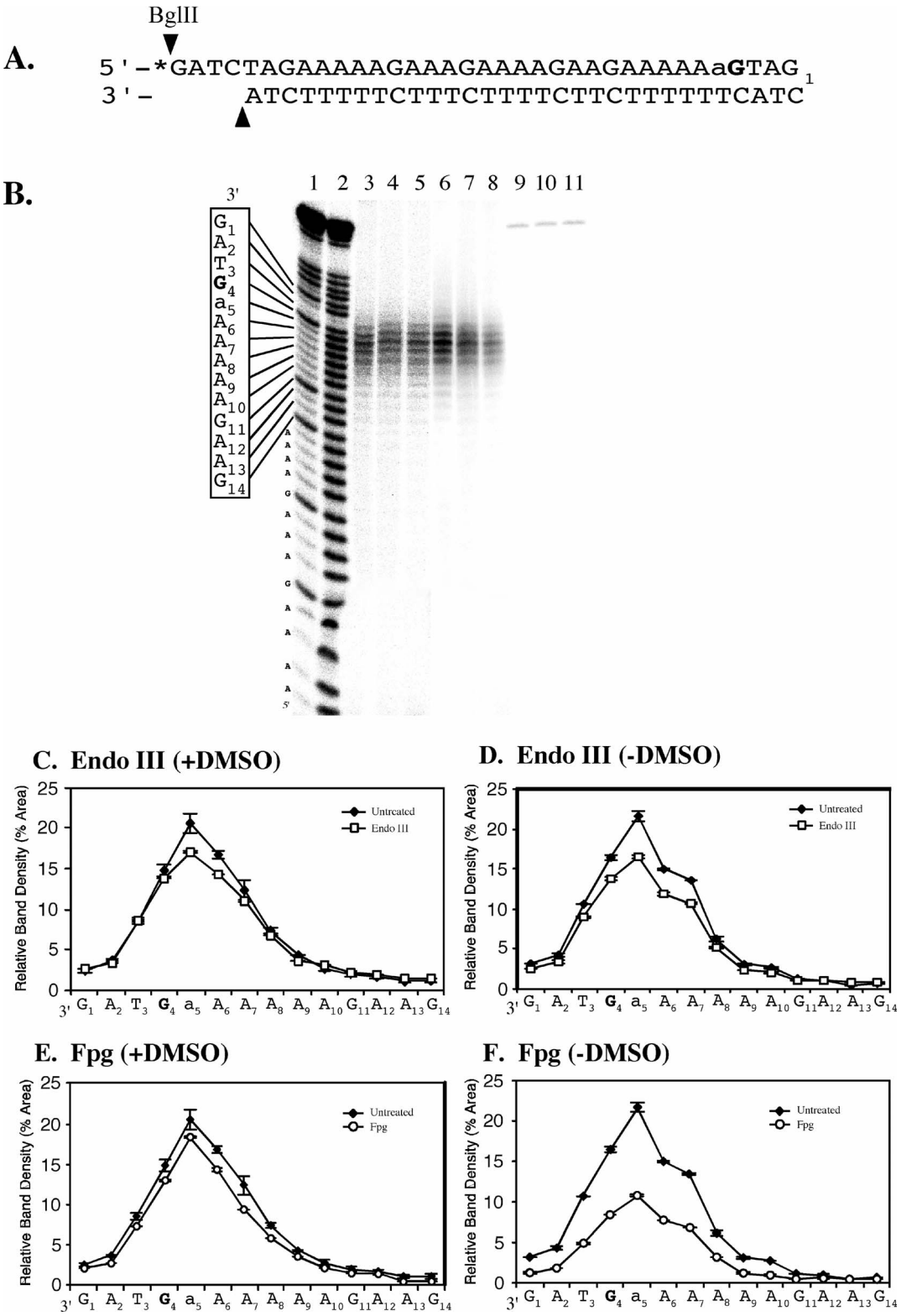


**FIG. 2.** Enzyme probing of the *Bgl*II fragment 5′-end labeled upper strand. Panel A: The *Bgl*II fragment model depicting the longest sequence detected. An asterisk indicates the 5′-$^{32}$P-end label, and the $^{125}$I-TFO targeted duplex G is in bold type. The subscripted number permits sequence correlation to those in panels B–F and Fig. 1. The lowercase ''a'' is the breakage maximum. Panel B: A typical 20% denaturing PAGE separation of DSB-terminated upper strands. Lanes 1 and 2, Maxam and Gilbert ''G'' and ''G+A'' sequencing ladders; lanes 3 and 6, $^{125}$I-DSB-terminated *Bgl*II fragments produced by irradiation (+) or (−) DMSO, respectively; lanes 4 and 7, endo III-treated *Bgl*II fragments (+) or (−) DMSO, respectively; lanes 5 and 8, Fpg-treated *Bgl*II fragments (+) or (−) DMSO respectively; lane 9, undamaged duplex 47-bp control fragment; lane 10, endo III-treated 47-bp control; lane 11, Fpg-treated 47-bp control. Bands representing breakpoints at nucleotides within the target sequence are numbered according to their position with respect to the longest fragment identified, counting up as the breaks progress toward the *Bgl*II restriction site. Panels C–F: Densi-

**TABLE 1**
**Densitometric Change after Enzyme Treatment**

| Irradiation condition | Density lost (%)[a] | | | |
|---|---|---|---|---|
| | Endo III-treated | | Fpg-treated | |
| | Upper strand | | Upper strand | |
| | 5′-end labeled | 3′-end labeled | 5′-end labeled | 3′-end labeled |
| (+) DMSO | 8.7 ± 0.1[b] | 14.3 ± 0.4[b] | 17.0 ± 0.3[c] | 21.4 ± 1.6[c] |
| (−) DMSO | 19.0 ± 1.1[c] | 13.9 ± 0.5[c] | 51 ± 0.3[b] | 30.8 ± 0.8[b] |
| | Lower strand | | Lower strand | |
| | 5′-end labeled | 3′-end labeled | 5′-end labeled | 3′-end labeled |
| (+) DMSO | 15.9 ± 1.4[c] | 23.6 ± 0.9[c] | 8.2 ± 1.9[b] | 10.9 ± 1.1[b] |
| (−) DMSO | 26.2 ± 1[b] | 35.9 ± 0.5[b] | 18 ± 1.8[b] | 13.2 ± 1.6[b] |

[a] Density lost is the mean percentage total density reduction in the enzyme-treated sample lanes of the gels with respect to the total density observed in the untreated damaged DNA control lanes.
[b] Percentages are shown ± the SEM for three independent determinations.
[c] Percentages are shown ± the SEM for two independent determinations.

(~19%) than for the (+) DMSO sample (~9%), indicating the presence of more endo III-sensitive sites after irradiation in the absence of DMSO (Table 1).

As expected for a purine-rich sequence, the 5′-end-labeled (+) DMSO sample exhibited nearly twofold greater sensitivity to cleavage by Fpg than by endo III (i.e. ~17% total density lost; Table 1). Also, the range of Fpg-sensitive fragments was much broader than that observed for endo III, spanning fragments $A_2$ through $A_9$ (Fig. 2E).

In contrast, the (−) DMSO sample was very sensitive to Fpg, displaying large decreases in density for nearly every fragment in the sample (Fig. 2F). More than half of all fragment density was lost (~51%) after Fpg digestion of the (−) DMSO sample, with those fragments closest to the DSB maximum again displaying the greatest enzyme sensitivity (Fig. 2F; Table 1). This suggests a high yield of upper-strand purine-derived lesions in association with and close to the DSBs formed during irradiation under non-scavenging conditions.

Fpg exhibits a range of effect and a level of cleavage activity for the (+) DMSO substrate that is similar to that of endo III for the (−) DMSO sample. This is consistent with the broader substrate specificity and greater activity of Fpg on purine-derived lesions and indicates purine damage when irradiation is performed under scavenging conditions (although at least a threefold lower yield than under unscavenged conditions; Table 1). Furthermore, with the exception of Fpg treatment of the (−) DMSO sample in which >50% of the fragments are cleaved, endo III and Fpg cleavage of the 5′-end-labeled upper strand is significantly less than that observed by endo IV treatment (*24*), indicating that the ability of these enzymes to recognize and cleave AP sites in these substrates is poor in comparison to endo IV. Therefore, cleavage by Fpg and endo III occurs predominantly at sites of base damage in these substrates.

### *Endo III and Fpg Probing of the 3′-End-Labeled Upper Strand*

The *Bgl*II fragments were 3′-end labeled by *Taq* DNA polymerase-mediated α-$^{32}$P-dATP incorporation as described previously (*24*). A subset (≤15%) of the *Bgl*II fragment DSB ends support labeling by *Taq* DNA polymerase and thus possess 3′-OH ends. This subset of upper-strand fragments exhibited very little endo III sensitivity, and only in fragments close to the DSB maximum (Fig. 3B and C). The Fpg digestion pattern was also similar to that obtained with the 5′-end-labeled upper strand in that the (−) DMSO sample exhibited more enzyme sensitivity and in a broader range of fragments than did the (+) DMSO sample (Fig. 3D and E). These results confirm the presence of purine-derived lesions close to the DSB maximum and the role of free radical processes in their formation.

### *Endo III and Fpg Probing of the 3′-End-Labeled Lower Strand*

As expected from its polypyrimidine sequence, the lower strand exhibits greater sensitivity to cleavage by endo III than by Fpg. As with Fpg treatment of the upper strand, endo III treatment of the polypyrimidinic lower strand reveals a greater lesion burden in the (−) DMSO sample than in the (+) DMSO sample (Fig. 4B and C; Table 1). Again, those fragments comprising the maximum DSB breakage

←

tometric quantification of sequencing gel bands representing breakpoints within the *Bgl*II fragment sequence. Panels C and D: Endo III-treated samples (+) and (−) DMSO respectively. Untreated *Bgl*II fragments (closed diamonds); endo III-treated fragments (open squares). Panels E and F: Fpg-treated samples (+) and (−) DMSO, respectively. Untreated *Bgl*II fragments (closed diamonds); Fpg-treated fragments (open circles). The points on the graphs represent the average percentage densitometric band area ± SEM for bands observed in three (panels C and E) or two experiments (panels D and F).

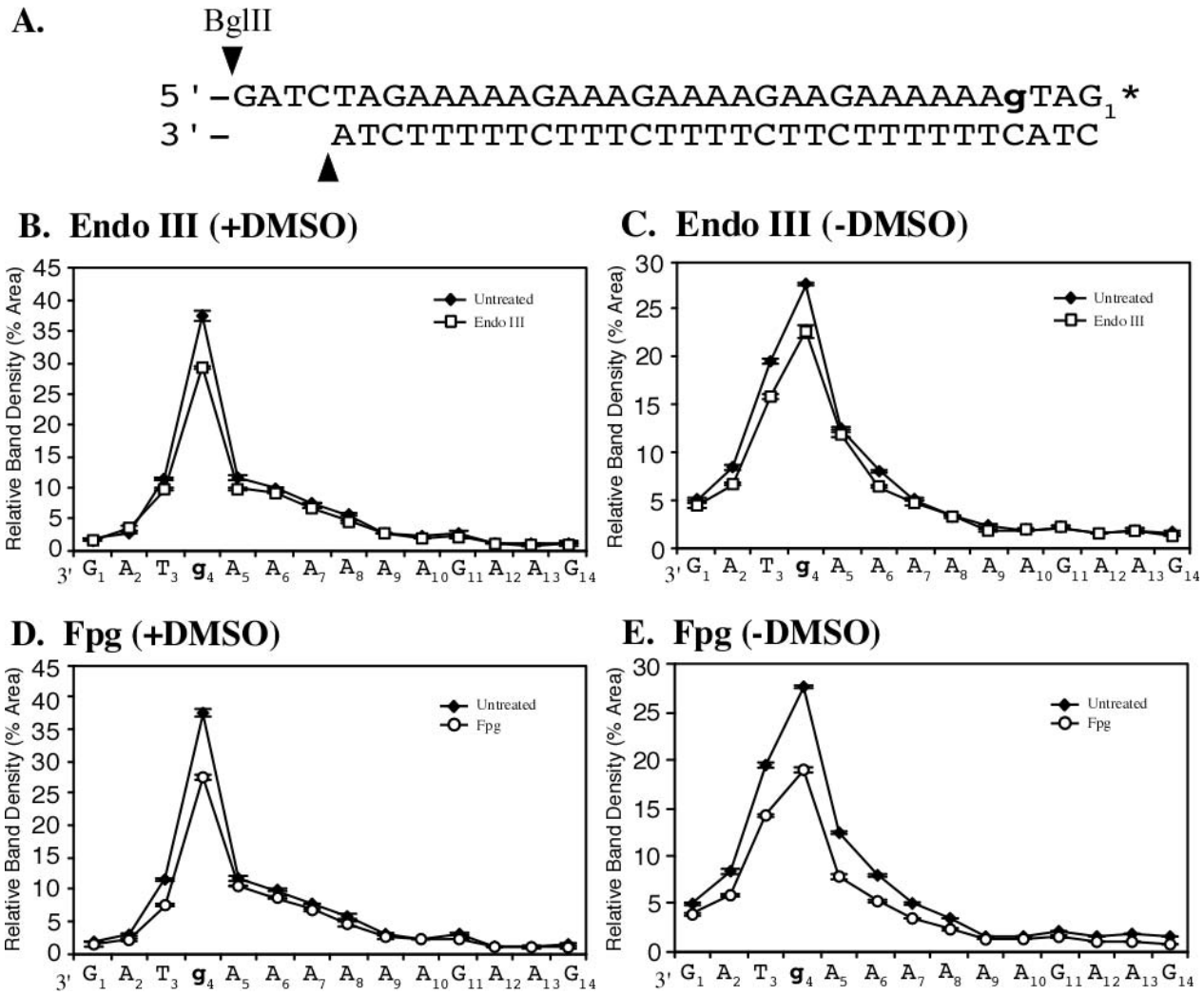


**FIG. 3.** Enzymatic probing of the *Bgl*II fragment 3′-end-labeled upper strand. Panel A: The *Bgl*II fragment model for the longest sequence detected. An asterisk indicates the 3′-$^{32}$P label. The $^{125}$I-TFO targeted duplex G (which is also the DSB breakage maximum) is indicated in lowercase bold type. The subscripted number permits correlation of this sequence to those in panels B–E and Fig. 1. Panels B–E: Densitometric quantification of sequencing gel bands representing breakpoints within the *Bgl*II fragment sequence. Panels B and C: Endo III-treated samples (+) and (−) DMSO, respectively. Untreated *Bgl*II fragments (closed diamonds); endo III-treated fragments (open squares). Panels D and E: Fpg-treated samples (+) and (−) DMSO, respectively. Untreated *Bgl*II fragments (closed diamonds); Fpg-treated fragments (open circles). The points on the graphs represent the average percentage densitometric band area ± SEM for bands observed in two (panels B and D) or three experiments (panels C and E).

exhibited the greatest enzymatic sensitivity (Fig. 4C). This result is consistent with our observations for the upper strand after irradiation in the absence of DMSO and helps to confirm the role of scavengeable free radicals in the formation of base lesions under these irradiation conditions. It also further supports our earlier observation that fragments terminating closest to the $^{125}$I decay site contain the most enzyme-recognizable lesions.

In contrast to endo III, the 3′-end-labeled lower strand fragments exhibit little sensitivity to Fpg. The overall Fpg sensitivity of the lower-strand (−) DMSO sample was slightly greater than that of the (+) DMSO sample (Fig. 4D and E; Table 1), and this finding is similar but complementary to our observations for endo III treatment of the 5′-end-labeled upper strand (Table 1).

### *Endo III and Fpg Probing of the 5′-End-Labeled Lower Strand*

As with upper strand DSB-damaged 3′-end labeling, labeling of the DSB-damaged 5′-end of the lower strand produces only a subset of labeled fragments, with the DSB maximum shifted to $T_6$ of the sequence as shown in Fig. 5. As discussed previously (*24*), this apparent shift in the DSB maximum is a function of the DSB end's capacity to support labeling by T4 PNK and is thus indicative of a fragment subset being labeled and not the true DSB maximum that is revealed by upper- and lower-strand end labeling at the *Bgl*II restriction cut end of the DSB-terminated fragments.

Endo III treatment of the 5′-end-labeled lower-strand fragments produces cleavage patterns in both (+) and (−)

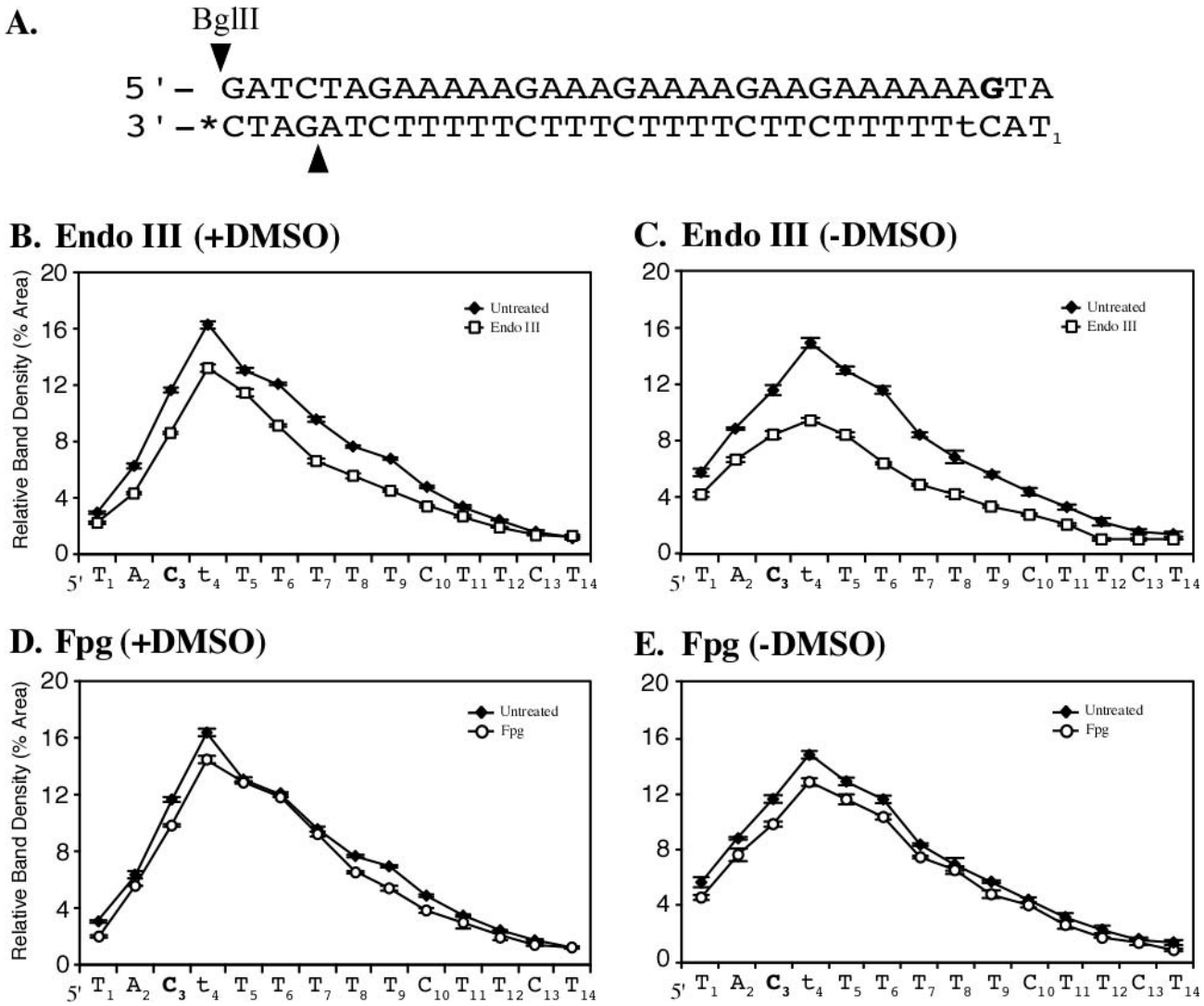


**FIG. 4.** Enzymatic probing of the *Bgl*II fragment 3′-end-labeled lower strand. Panel A: The *Bgl*II fragment model for the longest sequence detected. An asterisk indicates the 3′-$^{32}$P-end label, and the targeted G is shown in bold. The breakage maximum is indicated by a lowercase ''t''. Panels B–E: Densitometric quantification of sequencing gel bands representing breakpoints within the *Bgl*II fragment sequence. Panels B and C: Endo III-treated samples (+) and (−) DMSO, respectively. Untreated *Bgl*II fragments (closed diamonds); endo III-treated fragments (open squares). Panels D and E: Fpg-treated samples (+) and (−) DMSO, respectively. Untreated *Bgl*II fragments (closed diamonds); Fpg-treated fragments (open circles). The points on the graphs represent the average percentage densitometric band area ± SEM for bands observed in three experiments.

DMSO samples that are similar to those observed for the 3′-end-labeled lower strand (compare Fig. 5B and C and Fig. 4B and C). However, based on net density loss after endo III treatment, the sensitivity of these fragments is less than was observed for the 3′-end-labeled lower strand [~16% and ~26% compared to ~24% and ~36% for (+) and (−) DMSO samples respectively; Table 1], although still proportionately similar [i.e., ~1.5-fold more damage in the (−) DMSO samples]. Also, as with cleavage of the 3′-end-labeled upper-strand fragment subsets, cleavage of the lower-strand 5′-end-labeled fragment subset confirms base damage clustering near the DSB end. Again, as with all of the previous substrates, this lower-strand 5′-end-labeled fragment subset exhibits greater enzyme cleavage sensitivity in the (−) DMSO sample.

Consistent with the predominately pyrimidine sequence of the lower strand, and as observed previously with the 3′-end-labeled fragments, Fpg has limited ability to act on the 5′-end-labeled lower-strand fragments (Fig. 5D and E). However, as with the 3′-end-labeled lower-strand fragments, the (−) DMSO sample showed greater sensitivity to Fpg than the (+) DMSO sample (Table 1). This is consistent with the presence of more pyrimidine-derived lesions in the (−) DMSO sample, since Fpg may recognize and incise some pyrimidine-derived lesions to a limited extent (*32, 43*).

### *Base Damage Clustering is an $^{125}$I-DSB-Dependent Event*

The data obtained from enzymatic probing of the sequence immediately upstream from the $^{125}$I-induced DSB

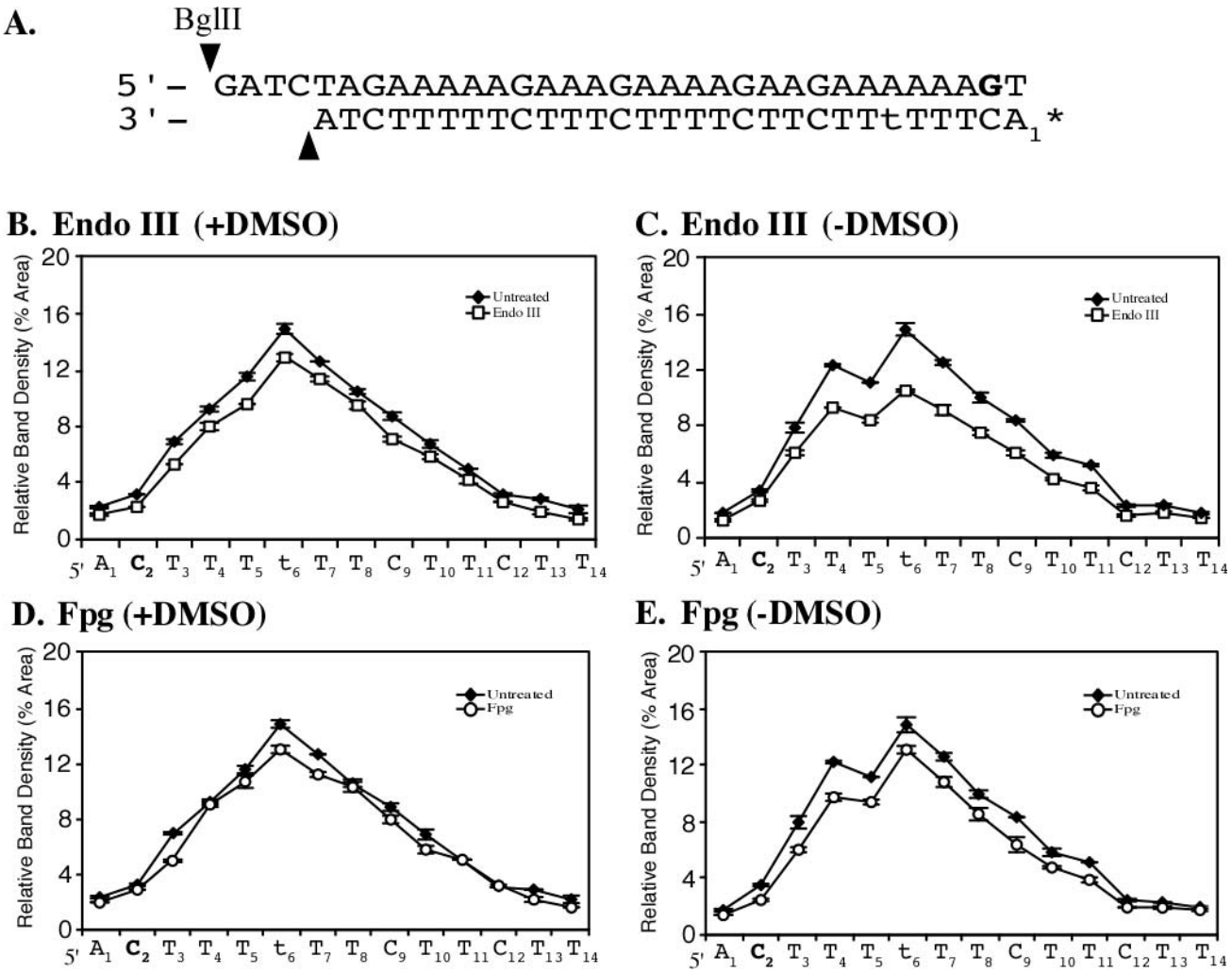


**FIG. 5.** Enzymatic probing of the *Bgl*II fragment 5′-end-labeled lower strand. Panel A: The *Bgl*II fragment model for the longest sequence detected. An asterisk indicates the 5′-$^{32}$P-end label, and the targeted G is shown in bold. The breakage maximum is indicated by a lowercase ''t''. Panels B–E: Densitometric quantification of sequencing gel bands representing breakpoints within the *Bgl*II fragment sequence. Panels B and C: Endo III-treated samples (+) and (−) DMSO, respectively. Untreated *Bgl*II fragments (closed diamonds); endo III-treated fragments (open squares). Panels D and E: Fpg-treated samples (+) and (−) DMSO, respectively. Untreated *Bgl*II fragments (closed diamonds); Fpg-treated fragments (open circles). The points on the graphs represent the average percentage densitometric band area ± SEM for bands observed in two (panels B and D) or three experiments (panels C and E).

suggest a high degree of base damage clustering, with ≥50% of the fragments formed within 8 bp of the DSB maximum containing base damage in their upper and lower strands. However, it is possible that the observed base damage is not a direct consequence of the decay event that formed the DSB but instead reflects nonspecific background damage produced by decay events occurring in surrounding plasmid/triplex molecules. If this were the case, the amount of base damage should be fairly uniform throughout the $^{125}$I-DSB linearized plasmid molecules. On the other hand, if the base damage clustering observed proximal to the $^{125}$I-induced DSBs were a direct consequence of the decays that formed the DSBs, internal sequences of the DSB-damaged linear plasmid should be less sensitive to cleavage by endo III and Fpg relative to the DSB terminated *Bgl*II fragments. To test this, we isolated a 49-bp internal control restriction fragment from 1354 bp upstream of the $^{125}$I-TFO target site in the $^{125}$I-linearized plasmids used to generate the *Bgl*II fragments used in the enzymatic probing experiments. The internal control fragments were essentially insensitive to cleavage by enzymatic base damage probing with endo III or Fpg (Fig. 6). This result demonstrates that the base damage clusters observed in proximity to the $^{125}$I-induced DSBs are a direct consequence of the decay events that produced the DSBs.

### *Identification of Specific Base Lesions Associated with $^{125}$I-DSBs*

Although enzymatic probing allows detection of base damage in the DNA sequence proximal to the $^{125}$I-TFO tar-

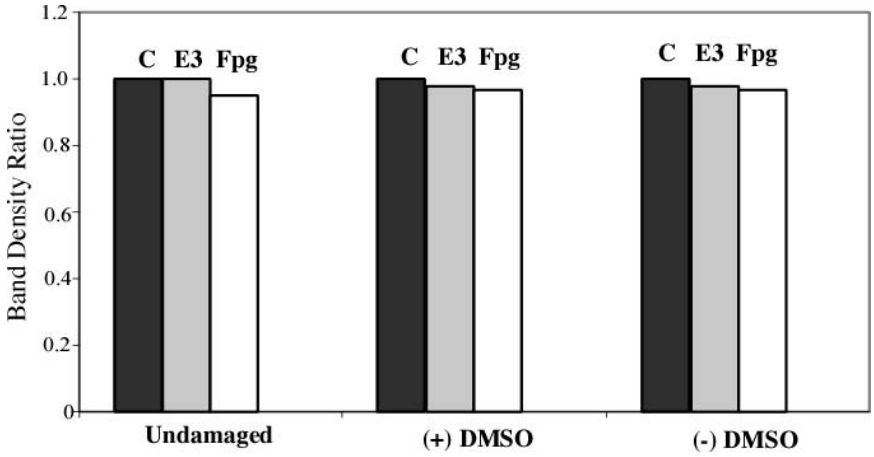


**FIG. 6.** Repair enzyme treatment of an internal control fragment. A 49-bp internal control restriction fragment recovered from the $^{125}$I-DSB linearized pTC27 plasmid [from (+) and (−) DMSO samples] by *Stu*I and *Sfi*I digestion was used to assess nonspecific background radiation damage by enzymatic probing with endo III and Fpg. Reactions were run under the same conditions described for repair enzyme probing of the DSB-terminated sample fragments [untreated control (C), endo III (E3), formamidopyrimidine-DNA glycosylase (Fpg)].

geted DSBs, it does not determine specific base lesion types due to the broad substrate specificity of the enzymes used. To identify specific base modifications, the *Bgl*II fragments isolated for the enzymatic probing experiments were subjected to analysis by gas chromatography/mass spectrometry (GC/MS). The (+) and (−) DMSO sample *Bgl*II fragment DNAs, as well as a control DNA fragment isolated from undamaged plasmid and corresponding to the sequence spanning the $^{125}$I-TFO target site of pTC27 between the *Bgl*II and *Mbi*I restriction sites (Fig. 1), were hydrolyzed and derivatized as described previously and analyzed by GC/MS (*38*). Three base lesions were identified. These were 8-hydroxyguanine (8-OH-Gua), 8-hydroxyadenine (8-OH-Ade), and 5-hydroxycytosine (5-OH-Cyt) (Fig. 7). The purine-derived lesions were present in greater relative yield than the pyrimidine-derived lesion, and this is consistent with our enzymatic probing results and the high sensitivity of purines to ionization and to oxidative damage (*44*). The yields of 8-OH-Ade and 8-OH-Gua were 1.5- and 1.3-fold greater, respectively, in the (−) DMSO samples. Although the proportional yield of 5-OH-Cyt was less than half that of 8-OH-Ade, and much less than half that of 8-OH-Gua in both (+) and (−) DMSO samples, its yield more than doubled (2.6-fold) in the absence of DMSO compared to that detected in the (+) DMSO sample. The molar ratio of G with respect to A in the target sequence is 1:4. Hence damage at G residues is much more frequent than damage at A residues.

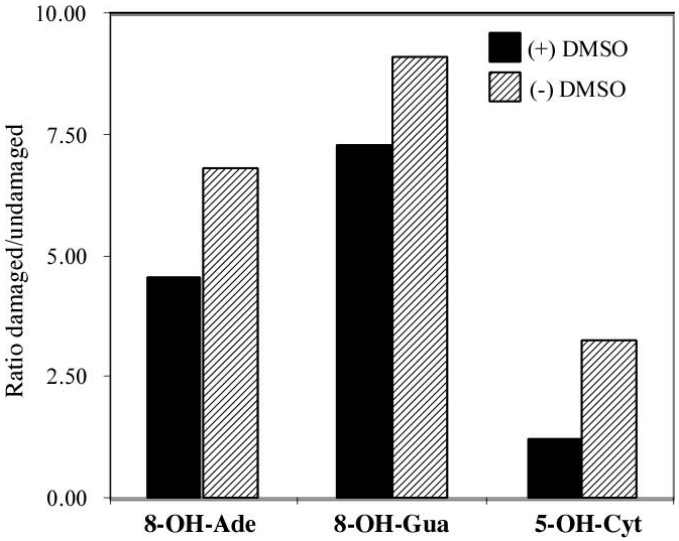


**FIG. 7.** Lesion identification. GC/MS analysis of base damage in the same DSB-terminated *Bgl*II restriction fragment samples used as substrates for repair enzyme probing of base damage. Results are expressed as the ratio of the lesion identified in the damaged DNA sample to the background observed in the undamaged control *Bgl*II/*Mbi*I DNA fragment (see Fig. 1). Three types of damage were detected: 8-OH-Ade, 8-OH-Gua and 5-OH-Cyt. 8-OH-Gua was detected in the highest amount in both samples tested. Larger amounts of each of the three lesion types were observed in the (−) DMSO samples compared to the (+) DMSO samples.

## DISCUSSION

Unlike oxidative processes, radiation produces temporally and spatially grouped ionizations that form molecular radicals in the medium with which it interacts. This unique mechanism of energy deposition leads to spatially clustered lesions [multiply damaged sites (MDS)] and was first proposed by Ward (*45, 46*). MDS have been predicted, and in some cases demonstrated (*47, 48*), to occur in numerous forms, including base damage in one or both DNA strands, combinations of base damage and single-strand breaks (SSBs), structurally simple DSBs, and complex DSBs in which various combinations of these lesions occur proximal to the break (*8*). Most of the cytotoxic effects attributed to radiation have been postulated to be due to radiation-induced DSBs, with the greater cytotoxicity of high-LET ra-

diation per lesion being ascribed to the higher likelihood of lesion clustering in proximity to the DSBs. Such DSBs are believed to be more refractory to repair than simple double-stranded discontinuities (*1, 49*). Our recent observations support the notion that non-DSB γ-radiation-induced damage (i.e. base damage and SSBs) upstream from a restriction enzyme-induced DSB is a potent inhibitor of human nonhomologous end joining (NHEJ) *in vitro* but not of simple direct ligation (*11*). Thus a clear understanding of the biochemical mechanisms responsible for radiation cytotoxicity and/or DSB repair cannot be achieved without a clear understanding of the structure of the lesion with which the DSB repair machinery must interact.

$^{125}$I-TFO targeting has allowed us to obtain DNA containing authentic radiation-induced DSBs within a known sequence context and perform molecular analysis of DSB-associated structural features. In a biological sense, the DSBs produced by $^{125}$I decay mimic those produced by high-LET beam irradiation, implying similar structural characteristics. However, unlike beam radiation, the $^{125}$I decay process results in essentially three modes of DNA damage induction. These are the direct and indirect low-LET radiation effects caused by the, on average, ~21 Auger electrons emitted by each decay, in conjunction with the non-radiation effects resulting from the charge transfers required from neighboring atoms to neutralize the $^{125}$Te daughter atom's net average +21 charge. All of these decay effects are highly temporally and spatially localized and thus lead to very localized DNA lesions in the form of DSBs and nucleotide damage proximal to the DSB ends in the duplex DNA's $^{125}$I-TFO-target sequence. Consequently, in addition to providing valuable insights into the radiobiological mechanisms and effects of $^{125}$I decay in DNA, this system my also be a good model for establishing general categories of structural features that are representative of complex radiation-induced DSBs.

A number of characteristics of these DSBs that do not directly involve damage proximal to the DSB ends have been described in detail elsewhere (*24*). Since the substrates used here are the same as those used previously, the general observations concerning the properties of the backbone discontinuities that comprise the DSB are also the same and will not be reiterated here.

The ''indirect'' and direct effects (including non-radiation effects) of radiation produced by $^{125}$I decay were differentiated by irradiating samples in the presence or absence of the free radical scavenger DMSO. Our observations show that the DSB yield (and AP site yield) was not affected by the presence or absence of DMSO, suggesting that most of the strand scission events are the result of direct effects and charge neutralization (*24*). These results are consistent with those reported previously by others (*25–29*). On the other hand, the yield of base damage in proximity to the DSB end was shown to be strongly affected by the presence or absence of DMSO during irradiation, with significantly more base damage being produced by irradiation in the absence of DMSO. Since irradiation occurs in the frozen state, this apparent ''indirect effect'' probably reflects damage caused by water radicals derived from the first hydration layer of the DNA rather than damage created by interaction of emitted electrons and/or electron stripping via charge neutralization directly in atoms and bonds of the target DNA. Thus this apparent DMSO scavenging effect may permit some differentiation between damage caused by direct energy deposition (and/or electron abstraction by charge neutralization) in the DNA and damage that results from secondary reactions with water radicals that are formed within the DNA's first hydration layer. As such, although some differentiation between modes of damage induction may be identifiable, based on current definitions, DNA damage in this irradiation system is produced primarily by direct effects.

Base damage proximal to the $^{125}$I-induced DSB end of the *Bgl*II restriction fragments was assessed by differential enzymatic probing using endo III and Fpg to identify pyrimidine- or purine-derived lesions, respectively. Although these enzymes are known to be capable of some crossover with regard to substrate specificity, kinetic and structure/function analyses of endo III and Fpg indicate that they will preferentially recognize their respective pyrimidine- or purine-derived substrates when presented with DNA containing a mixture of base lesions, particularly in irradiated DNA (*50–56*).

As expected from its polypurine sequence, the upper strand exhibited only limited sensitivity to endo III cleavage, and only at those fragments closest to the DSB maximum (Figs. 2 and 3). The relative increase in endo III sensitivity of the 5′-end-labeled upper strand fragments in the (−) DMSO sample with respect to those obtained in the (+) DMSO sample (Fig. 2C and D) suggests a role for scavengeable free radicals in the formation of endo III-recognizable base lesions in the (−) DMSO samples (Table 1). In contrast, although the breakage pattern differs, the fragment subset characterized by 3′-end labeling of the upper-strand (DSB damaged end) seems to display essentially equal overall sensitivity to cleavage by endo III (Table 1). This lack of an overall change in endo III sensitivity in the 3′-end-labeled upper-strand samples suggests that the endo III-recognizable base lesions closest to the DSB end in this fragment subset may be formed largely by direct energy deposition effects in the DNA and/or non-radiation ''hot atom'' mediated ionizations. If this is the case, and the effect is extrapolated to the larger pool of fragments represented by 5′-end labeling of the upper strand, we can speculate that the majority of base lesions produced by ''indirect effects'' (in this system this is most probably damage derived from water radicals produced in the DNA's first hydration layer) are likely to occur away from the $G_4$ residue targeted to hybridize with the $^{125}$I-dC of the TFO. Such a result would be consistent with the endo III cleavage sensitivity patterns observed in the 5′-end-labeled upper strand (Fig. 2C and D) and consistent with the strand break sen-

sitivity patterns observed for decay of $^{125}$I directly incorporated into short synthetic oligonucleotides as described by Lobachevsky and Martin (*28, 29*).

Fpg probing of the upper strands irradiated in the absence of DMSO (in particular the 5′-end-labeled upper strands) displayed the greatest enzyme sensitivity observed in this study, with >50% of the total fragment band density being lost after Fpg treatment (Table 1). In contrast, Fpg probing of the upper-strand fragments obtained from DNA irradiated in the presence of DMSO exhibited limited enzyme sensitivity, albeit more than for endo III in all respective samples. The increase in Fpg cleavage sensitivity displayed by the (−) DMSO sample relative to the (+) DMSO sample indicates a role for scavengeable free radicals in the formation of radiation-induced purine damage in this system (Table 1; Fig. 2E and F). Therefore, during irradiation in the absence of DMSO, the mechanism responsible for this effect is likely to involve first hydration layer derived ·OH addition to form purine C8-OH-adduct radicals, which subsequently undergo oxidation to form 8-OH-purine lesions (*57*). In contrast, when DMSO is present, ·OH are likely to be scavenged. Thus the mechanism may involve direct ionization either by the radiated Auger electrons and/or charge migration and electron stripping of atoms in the DNA duplex nucleobases to form purine radicals. Direct ionization mechanisms such as these would also form 8-OH-purines upon hydration and subsequent oxidation after thawing of the samples (*57*). Furthermore, those fragments that are most sensitive to Fpg cleavage are those representing the highest strand break frequency, with the DSB maximum (fragment $A_5$; Fig. 2F) and the two fragments upstream and downstream of this position displaying the greatest Fpg sensitivity. This observation further supports upper-strand base lesion clustering near the DSB end of the fragments.

As with the upper strand, endo III probing of the polypyrimidine lower strand (3′- and 5′-end labeled) reveals base damage, much of which can be attributed to scavengeable free radicals. In the 3′-end-labeled (+) DMSO samples, fragments $A_2$ to $C_{10}$ showed uniform density loss after endo III treatment (Fig. 4B), with a net total density loss of ~24% (Table 1). In contrast, endo III probing of the lower-strand (−) DMSO sample produced a different cleavage distribution pattern, with fragments $T_4$–$T_6$ displaying greater sensitivity to endo III, indicating an increased yield of free radical-mediated base damage in these fragments compared to the (+) DMSO sample (Fig. 4C). A similar DMSO-dependent endo III sensitivity response was seen in the fragments comprising the DSB breakage maxima observed by lower-strand 5′-end labeling (DSB damaged end; Fig. 5). Less total density was lost after endo III treatment of the 5′-end-labeled lower strand with respect to that observed by 3′-end labeling, indicating detection of a greater range of lesion-containing fragments after 3′-end labeling. As observed for the upper strand, the overall loss of fragment band density after endo III probing of the 5′-end-labeled lower strand points to base damage clustering near the DSB end (Table 1; Fig. 5B and C). However, although there do appear to be pyrimidine-derived lesions formed by scavengeable free radicals near the lower-strand DSB end, the yield appears to be less than half that of the purine-derived lesions produced in the upper strand. This result is consistent with the known nucleotide ionization sensitivities [G > A > C > T (*44*)], but it may also reflect a difference in the capacity of endo III and Fpg to recognize and cleave their respective substrates in the complex DSBs investigated here.

As discussed previously (*24*), in most of our experiments the electrophoresis conditions required to achieve the necessary resolution for the fragments comprising the DSB breakage spectrum resulted in a lower resolution limit of 9 nucleotides. In addition, our control reactions (Fig. 2, lanes 9–11, and data not shown) indicate that the enzyme preparations used in this work lack phosphatase and nonspecific nuclease activities, and the damaged plasmids did not exhibit high levels of nonspecific background damage due to the irradiation conditions (Fig. 6). However, significant losses in the total band density of the breakage spectrum were observed after enzymatic probing of the DSB-terminated restriction fragments (Table 1). Since the enzyme-dependent band density loss of the fragments comprising the breakage spectrum peak measured for the experiments depicted in Figs. 2–5 cannot be accounted for by the creation of new bands of shorter length or by a density shift from longer bands to shorter bands in the spectrum, lesions may exist within 9 bases of the $^{32}$P label at the fragment's ends. In the case of fragments labeled at the DSB end (upper and lower strands; Figs. 3 and 5), this result is not surprising and is consistent with base lesion clustering near the DSB. However, in the case of fragments labeled at the *Bgl*II cut end (Figs. 2 and 4), this result is somewhat unexpected. Taken together with the data obtained by labeling the fragment's DSB ends, these results suggest that the DNA contains base lesion clusters near the DSB end that decrease in frequency with distance from the $^{125}$I decay site (as does the breakage frequency) but then increase in frequency again at distances greater than 24 bases upstream from the decay site. A similar enzymatic sensitivity pattern was observed for these substrates when they were probed for AP sites using endo IV (*24*). To determine whether this interpretation of our data is correct, we sought to establish electrophoresis conditions that would permit concurrent observation of fragments less than 9 nucleotides in length while still maintaining sufficient resolution at the position of the $^{125}$I-decay target sequence to identify the fragments defining the DSB induction spectrum. Establishing such conditions permits direct observation of enzyme-dependent formation of short fragments representing induction of base damage at a distance from the $^{125}$I decay site. The results of one such experiment are illustrated in Fig. 8. As can be seen, Fpg treatment of the upper-strand $^{32}$P-5′-end-labeled *Bgl*II fragment results in the production of fragments that

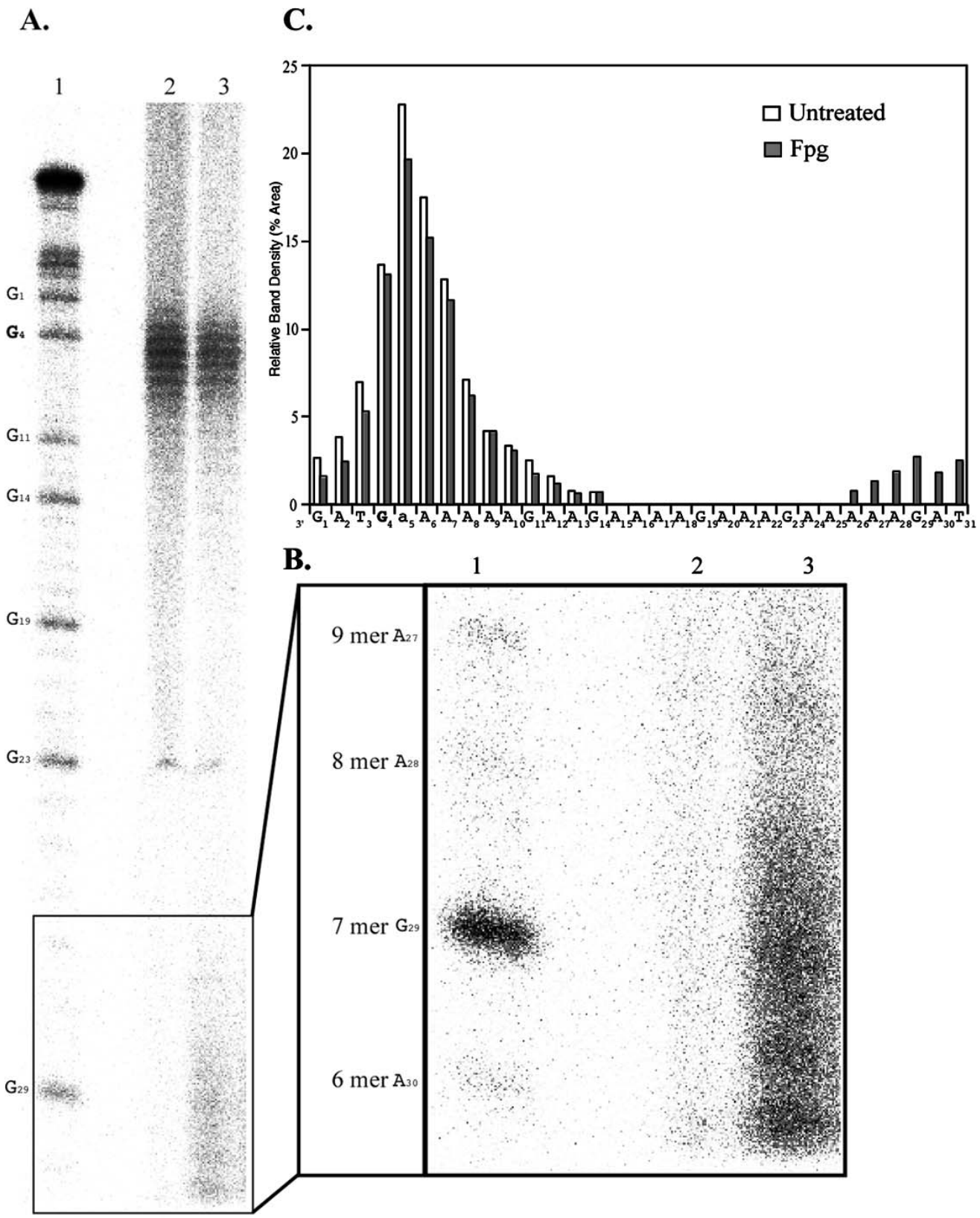


**FIG. 8.** Identification of increasing base damage frequencies at sites more than 24 nucleotides upstream from the initial $^{125}$I decay site. Panel A: Denaturing polyacrylamide gel (20%) showing changes in band densities and formation of short fragments after Fpg treatment of the 5′-$^{32}$P-labeled DSB-containing *Bgl*II fragment. Lane 1, Maxam and Gilbert sequencing ladder for G; lane 2, untreated DSB-terminated *Bgl*II fragments; lane 3, Fpg-treated DSB-terminated *Bgl*II fragments. The sequencing ladder is labeled at G's, and $G_1$ represents the longest fragment population observed after DSB induction by $^{125}$I decay and *Bgl*II cleavage. Panel B: Magnified and contrast-enhanced lower portion of the gel showing Fpg cleavage-dependent

predominately have lengths of 7 nucleotides or less (Fig. 8A and B). This unusual base damage distribution pattern might be explained by charge migration from base lesions produced near the DSB ends to the G residue (and bases in its proximity) that terminate the polypurine sequence of the TFO binding site. As discussed previously (*24*), such a speculation does seem to be consistent with the likely charge migration characteristics of the upper-strand sequence (*58*) and would appear to be supported by our data.

Based on the known limitations of the enzymes used in this study [with respect to cleavage at sites in which two lesions are closely opposed on opposite strands (*59*)], the enzymatic probing analysis suggests a conservative estimate of at least 50% of the upper and lower strands of the $^{125}$I-DSB terminated *Bgl*II restriction fragments being likely to contain some form of base damage. Furthermore, many of these fragments are likely to contain multiple lesions. The majority of base lesions in these substrates are likely to occur within 8 bases of the DSB end, and they are a direct consequence of the decays responsible for forming the DSBs. This conclusion is based on the lack of increased sensitivity to enzymatic probing of the 49-bp internal control restriction fragment isolated from the irradiated plasmids compared to the same fragment isolated from unirradiated plasmid (Fig. 6).

Finally, GC/MS analysis of the DSB terminated *Bgl*II restriction fragments allowed us to identify three specific base lesions that exist within this region. These lesions are 8-hydroxyguanine, 8-hydroxyadenine and 5-hydroxycytosine. The lack of thymine-derived lesions is consistent with the low yield of lesions detected by endo III probing of the lower strand fragments. This finding is further supported by the absence of detectable thymine glycol after $^{32}$P postlabeling analysis of the *Bgl*II fragments (data not shown).

This work, together with our work on AP site clustering in this system (*24*), allows us to begin construction of a model for the structural organization of a complex radiation-induced DSB. Additional studies to quantitatively assess individual lesion yields within this sequence will permit the development of a probability map for the locations of individual base lesions. This approach should allow us to improve the resolution of our model. However, even without this type of additional analysis, the data we have generated can be used to construct synthetic DSB substrates and develop a more refined analysis of the effect DSB structure has on the biochemical mechanisms involved in DSB repair.

## ACKNOWLEDGMENTS

This research was supported in part by the Intramural Research Program of the NIH through the Warrren Grant Magnuson Clinical Center. Certain commercial equipment or materials are identified in this paper to specify the experimental procedure adequately. Such identification does not imply recommendation or endorsement by the National Institute of Standards and Technology, nor does it imply that the materials or equipment identified are necessarily the best available for the purpose.

Received: March 20, 2006; accepted: July 26, 2006

## REFERENCES

*1.* J. F. Ward, The complexity of DNA-damage: Relevance to biological consequences. *Int. J. Radiat. Biol.* **66**, 427–432 (1994).

*2.* C. Badie, G. Iliakis, N. Foray, G. Asbeih, B. Cedervall, N. Chavaudra, G. Pantelias, C. Arlett and E. Malaise, Induction and rejoining of DNA double-strand breaks and interphase chromosome breaks after exposure to X rays in one normal and two hypersensitive human fibroblast cell lines. *Radiat. Res.* **144**, 26–35 (1995).

*3.* N. Foray, A. Priestley, G. Alsbeih, C. Badie, E. P. Capulas, C. F. Arlett and E. P. Malaise, Hypersensitivity of ataxia telangiectasia fibroblasts to ionizing radiation is associated with a repair deficiency of DNA double-strand breaks. *Int. J. Radiat. Biol.* **72**, 271–283 (1997).

*4.* R. B. Painter, B. R. Young and H. J. Burki, Non-repairable strand breaks induced by $^{125}$I incorporated into mammalian DNA. *Proc. Natl. Acad. Sci. USA* **71**, 4836–4838 (1974).

*5.* R. E. Krisch, F. Krasin and C. J. Sauri, DNA breakage, repair and lethality after $^{125}$I decay in rec+ and recA strains of *Escherichia coli*. *Int. J. Radiat. Biol. Relat. Stud. Phys. Chem. Med.* **29**, 37–50 (1976).

*6.* D. Blocher, DNA double-strand break repair determines the RBE of alpha-particles. *Int. J. Radiat. Biol.* **54**, 761–771 (1988).

*7.* S. B. Curtis, Lethal and potentially lethal lesions induced by radiation: A unified repair model. *Radiat. Res.* **106**, 252–270 (1986).

*8.* J. F. Ward, DNA damage produced by ionizing-radiation in mammalian-cells-identities, mechanisms of formation, and reparability. *Prog. Nucleic Acid Res. Mol. Biol.* **35**, 95–125 (1988).

*9.* P. L. Olive, The role of DNA single- and double-strand breaks in cell killing by ionizing radiation. *Radiat. Res.* **150** (Suppl.), S42–S51 (1998).

*10.* S. J. Dibiase, Z. C. Zeng, R. Chen, T. Hyslop, W. J. Curran and G. Iliakis, DNA-dependent protein kinase stimulates an independently active, nonhomologous, end-joining apparatus. *Cancer Res.* **60**, 1245–1253 (2000).

*11.* E. Pastwa, R. D. Neumann, K. Mezhevaya and T. A. Winters, Repair of radiation-induced DNA double-strand breaks is dependent upon radiation quality and the structural complexity of double-strand breaks. *Radiat. Res.* **159**, 251–261 (2003).

*12.* M. A. Hill, M. T. Herdman, D. L. Stevens, N. J. Jones, J. Thacker and D. T. Goodhead, Relative sensitivities of repair-deficient mammalian cells for clonogenic survival after alpha-particle irradiation. *Radiat. Res.* **162**, 667–676 (2004).

*13.* J. Drouet, C. Delteil, J. Lefrancois, P. Concannon, B. Salles and P. Calsou, DNA-dependent protein kinase and XRCC4-DNA ligase IV mobilization in the cell in response to DNA double strand breaks. *J. Biol. Chem.* **280**, 7060–7069 (2005).

*14.* E. Riballo, M. Kuhne, N. Rief, A. Doherty, G. C. M. Smith, M. J.

←

accumulation of small fragments. The estimated size of the fragments and their corresponding position on the sequence are shown in the side bar. Lane notations are the same as in panel A. Panel C: Graphical representation of the loss and gain of the fragments observed in panel A, lanes 2 and 3. The $G_4$ shown in bold represents the base targeted for Hoogsteen base pairing by the $^{125}$I-dC of the $^{125}$I-TFO, and the lowercase ''a'' represents the DSB breakage frequency maximum.

Recio, C. Reis, K. Dahm, A. Fricke and A. Krempler, A pathway of double-strand break rejoining dependent upon ATM, artemis, and proteins locating to gamma-H2AX foci. *Mol. Cell* **16**, 715–724 (2004).

*15.* S. E. Critchlow and S. P. Jackson, DNA-end-joining: From yeast to man. *Trends Biochem. Sci.* **23**, 394–398 (1998).

*16.* P. A. Jeggo, Identification of genes involved in repair of DNA double-strand breaks in mammalian cells. *Radiat. Res.* **150** (Suppl.), S80–S91 (1998).

*17.* E. C. Friedberg, G. C. Walker and W. Siede, *DNA Repair and Mutagenesis.* ASM Press, Washington, DC, 1995.

*18.* I. G. Panyutin and R. D. Neumann, Sequence-specific DNA double-strand breaks induced by triplex forming $^{125}$I labeled oligonucleotides. *Nucleic Acids Res.* **22**, 4979–4982 (1994).

*19.* I. G. Panyutin and R. D. Neumann, Sequence-specific DNA breaks produced by triplex-directed decay of iodine-125. *Acta Oncol.* **35**, 817–823 (1996).

*20.* I. G. Panyutin, T. A. Winters, L. E. Feinendegen and R. D. Neumann, Development of DNA-based radiopharmaceuticals carrying Auger-electron emitters for anti-gene radiotherapy. *Q. J. Nucl. Med.* **44**, 256–267 (2000).

*21.* R. F. Martin and W. A. Haseltine, Range of radiochemical damage to DNA with decay of iodine-125. *Science* **213**, 896–898 (1981).

*22.* A. I. Kassis, K. S. Sastry and S. J. Adelstein, Kinetics of uptake, retention, and radiotoxicity of $^{125}$IUdR in mammalian cells: Implications of localized energy deposition by Auger processes. *Radiat. Res.* **109**, 78–89 (1987).

*23.* O. A. Sedelnikova, I. G. Panyutin, A. R. Thierry and R. D. Neuman, Radiotoxicity of iodine-125-labeled oligodeoxyribonucleotides in mammalian cells. *J. Nucl. Med.* **39**, 1412–1418 (1998).

*24.* K. Datta, R. D. Neumann and T. A. Winters, Characterization of complex apurinic/apyrimidinic site clustering associated with an authentic radiation-induced DNA double-strand break. *Proc. Natl. Acad. Sci. USA* **102**, 10569–10574 (2005).

*25.* W. B. Li, W. Friedland, P. Jacob, I. G. Panyutin and H. G. Paretzke, Simulation of I-125 decay in a synthetic oligodeoxynucleotide with normal and distorted geometry and the role of radiation and non-radiation actions. *Radiat. Environ. Biophys.* **43**, 23–33 (2004).

*26.* I. S. Kandaiya, P. N. Lobachevsky, G. Dcunha and R. F. Martin, DNA strand breakage by I-125-decay in a synthetic oligodeoxynucleotide. 1. Fragment distribution and evaluation of DMSO protection effect. *Acta Oncol.* **35**, 803–808 (1996).

*27.* P. N. Lobachevsky and R. F. Martin, DNA strand breakage by I-125-decay in a synthetic oligodeoxynucleotide. 2. Quantitative analysis of fragment distribution. *Acta Oncol.* **35**, 809–815 (1996).

*28.* P. N. Lobachevsky and R. F. Martin, Iodine-125 decay in a synthetic oligodeoxynucleotide. I. Fragment size distribution and evaluation of breakage probability. *Radiat. Res.* **153**, 263–270 (2000).

*29.* P. N. Lobachevsky and R. F. Martin, Iodine-125 decay in a synthetic oligodeoxynucleotide. II. The role of Auger electron irradiation compared to charge neutralization in DNA breakage. *Radiat. Res.* **153**, 271–278 (2000).

*30.* S. Boiteux, Properties and biological functions of the NTH and FPG proteins of *Escherichia coli*: Two DNA glycosylases that repair oxidative damage in DNA. *J. Photochem. Photobiol. B* **19**, 87–96 (1993).

*31.* M. Dizdaroglu, J. Laval and S. Boiteux, Substrate specificity of the *Escherichia coli* endonuclease III: Excision of thymine- and cytosine-derived lesions in DNA produced by radiation-generated free radicals. *Biochemistry* **32**, 12105–12111 (1993).

*32.* Z. Hatahet, Y. W. Kow, A. A. Purmal, R. P. Cunningham and S. S. Wallace, New substrates for old enzymes: 5-hydroxy-2′-deoxycytidine and 5-hydroxy-2′-deoxyuridine are substrates for *Escherichia coli* endonuclease-III and formamidopyrimidine DNA N-glycosylase, while 5-hydroxy-2′-deoxyuridine is a substrate for uracil DNA N-glycosylase. *J. Biol. Chem.* **269**, 18814–18820 (1994).

*33.* M. Dizdaroglu, C. Bauche, H. Rodriguez and J. Laval, Novel substrates of *Escherichia coli* Nth protein and its kinetics for excision of modified bases from DNA damaged by free radicals. *Biochemistry* **39**, 5586–5592 (2000).

*34.* S. Boiteux, E. Gajewski, J. Laval and M. Dizdaroglu, Substrate specificity of the *Escherichia coli* Fpg protein (formamidopyrimidine-DNA glycosylase): Excision of purine lesions in DNA produced by ionizing radiation or photosensitization. *Biochemistry* **31**, 106–110 (1992).

*35.* K. Mezhevaya, T. A. Winters and R. D. Neumann, Gene targeted DNA double-strand break induction by $^{125}$I-labeled triplex-forming oligonucleotides is highly mutagenic following repair in human cells. *Nucleic Acids Res.* **27**, 4282–4290 (1999).

*36.* K. Datta, R. D. Neumann and T. A. Winters, A protocol for separation and isolation of small and/or large DNA fragments with high yield using CL4B Sepharose. *Anal. Biochem.* **317**, 284–287 (2003).

*37.* M. Dizdaroglu, P. Jaruga, M. Birincioglu and H. Rodriguez, Free radical-induced damage to DNA: Mechanisms and measurement. *Free Radic. Biol. Med.* **32**, 1102–1115 (2002).

*38.* M. Dizdaroglu, Measurement of oxidative DNA damage by gas chromatography-mass spectrometry and liquid chromatography-mass spectrometry. In *Sample Preparation for Hyphenated Analytical Techniques* (J. M. Rosenfeld, Ed.), pp. 39–51. CRC Press, London, 2004.

*39.* V. Bailly and W. G. Verly, *Escherichia coli* endonuclease III is not an endonuclease but a beta-elimination catalyst. *Biochem. J.* **242**, 565–572 (1987).

*40.* Y. W. Kow and S. S. Wallace, Mechanism of action of *Escherichia coli* endonuclease-III. *Biochemistry* **26**, 8200–8206 (1987).

*41.* J. Tchou, H. Kasai, S. Shibutani, M. H. Chung, J. Laval, A. P. Grollman and S. Nishimura, 8-Oxoguanine (8-hydroxyguanine) DNA glycosylase and its substrate-specificity. *Proc. Natl. Acad. Sci. USA* **88**, 4690–4694 (1991).

*42.* J. Tchou and A. P. Grollman, The catalytic mechanism of Fpg protein: Evidence for a Schiff-base intermediate and amino-terminus localization of the catalytic site. *J. Biol. Chem.* **270**, 11671–11677 (1995).

*43.* S. S. Wallace, Enzymatic processing of radiation-induced free radical damage in DNA. *Radiat. Res.* **150** (Suppl.), S60–S79 (1998).

*44.* S. Steenken and S. V. Jovanovic, How easily oxidizable is DNA? One-electron reduction potentials of adenosine and guanosine radicals in aqueous solution. *J. Am. Chem. Soc.* **119**, 617–618 (1997).

*45.* J. F. Ward, Some biochemical consequences of the spatial-distribution of ionizing radiation-produced free-radicals. *Radiat. Res.* **86**, 185–195 (1981).

*46.* J. F. Ward, Biochemistry of DNA lesions. *Radiat. Res.* **104** (Suppl.), S103–S111 (1985).

*47.* A. G. Georgakilas, P. V. Bennett, D. M. Wilson and B. M. Sutherland, Processing of bistranded abasic DNA clusters in gamma-irradiated human hematopoietic cells. *Nucleic Acids Res.* **32**, 5609–5620 (2004).

*48.* N. Yang, H. Galick and S. S. Wallace, Attempted base excision repair of ionizing radiation damage in human lymphoblastoid cells produces lethal and mutagenic double strand breaks. *DNA Repair* **3**, 1323–1334 (2004).

*49.* J. F. Ward, Complexity of damage produced by ionizing radiation. *Cold Spring Harb. Symp. Quant. Biol.* **65**, 377–382 (2000).

*50.* T. Melvin, S. Cunniffe, D. Papworth, T. Roldan-Arjona and P. O'Neill, Irradiation of DNA with 193 nm light yields formamidopyrimidine-DNA glycosylase (Fpg) protein-sensitive lesions. *Photochem. Photobiol.* **65**, 660–665 (1997).

*51.* T. Melvin, S. M. Cunniffe, P. O'Neill, A. W. Parker and T. Roldan-Arjona, Guanine is the target for direct ionisation damage in DNA, as detected using excision enzymes. *Nucleic Acids Res.* **26**, 4935–4942 (1998).

*52.* K. M. Prise, C. H. L. Pullar and B. D. Michael, A study of endonuclease III-sensitive sites in irradiated DNA: Detection of alpha-particle-induced oxidative damage. *Carcinogenesis* **20**, 905–909 (1999).

*53.* B. M. Sutherland, P. V. Bennett, O. Sidorkina and J. Laval, Clustered DNA damages induced in isolated DNA and in human cells by low

doses of ionizing radiation. *Proc. Natl. Acad. Sci. USA* **97**, 103–108 (2000).

*54.* M. Gulston, J. Fulford, T. Jenner, C. de Lara and P. O'Neill, Clustered DNA damage induced by radiation in human fibroblasts (HF19), hamster (V79-4) cells and plasmid DNA is revealed as Fpg and Nth sensitive sites. *Nucleic Acids Res.* **30**, 3464–3472 (2002).

*55.* J. Cadet, T. Douki, D. Gasparutto and J. L. Ravanat, Oxidative damage to DNA: Formation, measurement and biochemical features. *Mutat. Res.* **531**, 5–23 (2003).

*56.* M. Dizdaroglu, Substrate specificities and excision kinetics of DNA glycosylases involved in base-excision repair of oxidative DNA damage. *Mutat. Res.* **531**, 109–126 (2003).

*57.* M. D. Evans, M. Dizdaroglu and M. S. Cooke, Oxidative DNA damage and disease: Induction, repair and significance. *Mutat. Res.* **567**, 1–61 (2004).

*58.* P. O'Neill, A. W. Parker, M. A. Plumb and L. D. A. Siebbeles, Guanine modifications following ionization of DNA occurs predominantly via intra- and not interstrand charge migration: An experimental and theoretical study. *J. Phys. Chem. B* **105**, 5283–5290 (2001).

*59.* M. Weinfeld, A. Rasouli-Nia, M. A. Chaudhry and R. A. Britten, Response of base excision repair enzymes to complex DNA lesions. *Radiat. Res.* **156**, 584–589 (2001).